

Current Biology

Linear Self-Motion Cues Support the Spatial Distribution and Stability of Hippocampal Place Cells

Highlights

- Place fields from *tilted* place cells have reduced spatial coherence
- Most place fields from *tilted* mice form near environmental boundaries
- *Tilted* place cells show decreased stability across standard recording sessions

Authors

Ryan E. Harvey, Stephanie A. Rutan, Gabrielle R. Willey, Jennifer J. Siegel, Benjamin J. Clark, Ryan M. Yoder

Correspondence

ryoder@coastal.edu

In Brief

Harvey et al. describe how place cells from otoconia-deficient mice become unstable across sessions and show a tendency to form place fields along environmental boundaries.



Linear Self-Motion Cues Support the Spatial Distribution and Stability of Hippocampal Place Cells

Ryan E. Harvey,^{1,2} Stephanie A. Rutan,¹ Gabrielle R. Willey,¹ Jennifer J. Siegel,³ Benjamin J. Clark,² and Ryan M. Yoder^{1,4,5,*}

¹Department of Psychology, Indiana University-Purdue University Fort Wayne, Fort Wayne, IN 46805, USA

²Department of Psychology, University of New Mexico, Albuquerque, NM 87131, USA

³Center for Learning and Memory, The University of Texas, Austin, TX 78712, USA

⁴Present address: Department of Psychology, Coastal Carolina University, PO Box 261954, Conway, SC 29528-6054, USA

⁵Lead Contact

*Correspondence: ryoder@coastal.edu

<https://doi.org/10.1016/j.cub.2018.04.034>

SUMMARY

The vestibular system provides a crucial component of place-cell and head-direction cell activity [1–7]. Otolith signals are necessary for head-direction signal stability and associated behavior [8, 9], and the head-direction signal's contribution to parahippocampal spatial representations [10–14] suggests that place cells may also require otolithic information. Here, we demonstrate that self-movement information from the otolith organs is necessary for the development of stable place fields within and across sessions. Place cells in otoconia-deficient *tilted* mice showed reduced spatial coherence and formed place fields that were located closer to environmental boundaries, relative to those of control mice. These differences reveal an important otolithic contribution to place-cell functioning and provide insight into the cognitive deficits associated with otolith dysfunction.

RESULTS AND DISCUSSION

Basic Firing Characteristics in *Tilted* Mice Were Slightly Altered

We evaluated place-cell activity in *tilted* and control mice across five consecutive sessions (standard, cue rotation, standard, dark, standard) outlined in Figure 1A. To assess the degree to which place fields are anchored to environmental landmarks, session 2 involved a 90° cue rotation and session 4 was a dark trial, thereby limiting visual input and increasing reliance on internal self-motion.

We first investigated the impact of otoconia deficiency on basic firing measures of place cells in session 1. Place cells from *tilted* mice exhibited higher peak firing rates, lower spatial coherence, smaller field widths, and higher outfield firing rates than place cells from control mice (all $p < .038$), while average firing rates, number of active bins, sparsity, spatial information content, and infield firing rates were similar between groups, (all $p > 0.09$; Table S1).

Tilted place cells had higher peak firing rates overall, compared with control mice ($F(1,146) = 6.96$, $p = 0.009$, Figure 1C). It is possible that increased running speed in *tilted* mice accounts for their higher firing rates, as demonstrated previously [15]. However, the opposite pattern was observed—while control and *tilted* groups had similar correlations between firing rate and running speed ($t(147) = -1.08$, $p = 0.283$), control mice had greater speeds compared to *tilted* mice ($t(151) = 5.00$, $p < 0.001$, CI [95% confidence interval] [0.82, 1.90], $d = 0.70$). Thus, higher firing rates in *tilted* mice were not associated with increased running speed.

Many neurons in the hippocampus are theta modulated [16]. We determined the extent of theta modulation in our sample by computing spike-train temporal autocorrelations for individual cells in session 1 and examined the degree of modulation by computing a theta index [17]. Control and *tilted* cells were similarly modulated by theta ($Z = 0.09$, $p = 0.927$), and theta-modulated cells from both groups shared similar peak theta frequencies, ($t(56) = 1.2$, $p = 0.237$; Figure S3), which suggests that differences observed in *tilted* mice may not be due to differences in theta modulation.

Spatial Specificity and Coherence of Place-Cell Firing in *Tilted* Mice

Tilted mice lack otolithic representation of linear acceleration and may have deficits in accurately perceiving their velocity, thus resulting in abnormal firing fields. Accordingly, field widths, defined as contiguous bins where the cell fired $\geq 20\%$ of its peak rate, were smaller for the *tilted* group than for the controls ($F(1,146) = 10.6$, $p = 0.001$; Figure 1D). Despite the smaller field widths in the *tilted* group, the number of active bins, defined as the total number of bins $\geq 20\%$ of the peak rate, were similar between groups ($F(1,146) = 1.72$, $p = 0.19$; Table S1). The combination of smaller field widths and equal numbers of active bins suggests that the contiguity, or smoothness, of place fields might be disrupted in *tilted* mice. As expected, *tilted* mice showed decreased spatial coherence compared to controls overall ($F(1,137) = 36.99$, $p < 0.001$; Figure 1E), similar to findings in rats with complete vestibular inactivation [4]. Figure 1B illustrates place-field examples from control and *tilted* mice, and Figure S2 illustrates where these examples reside in respect to our



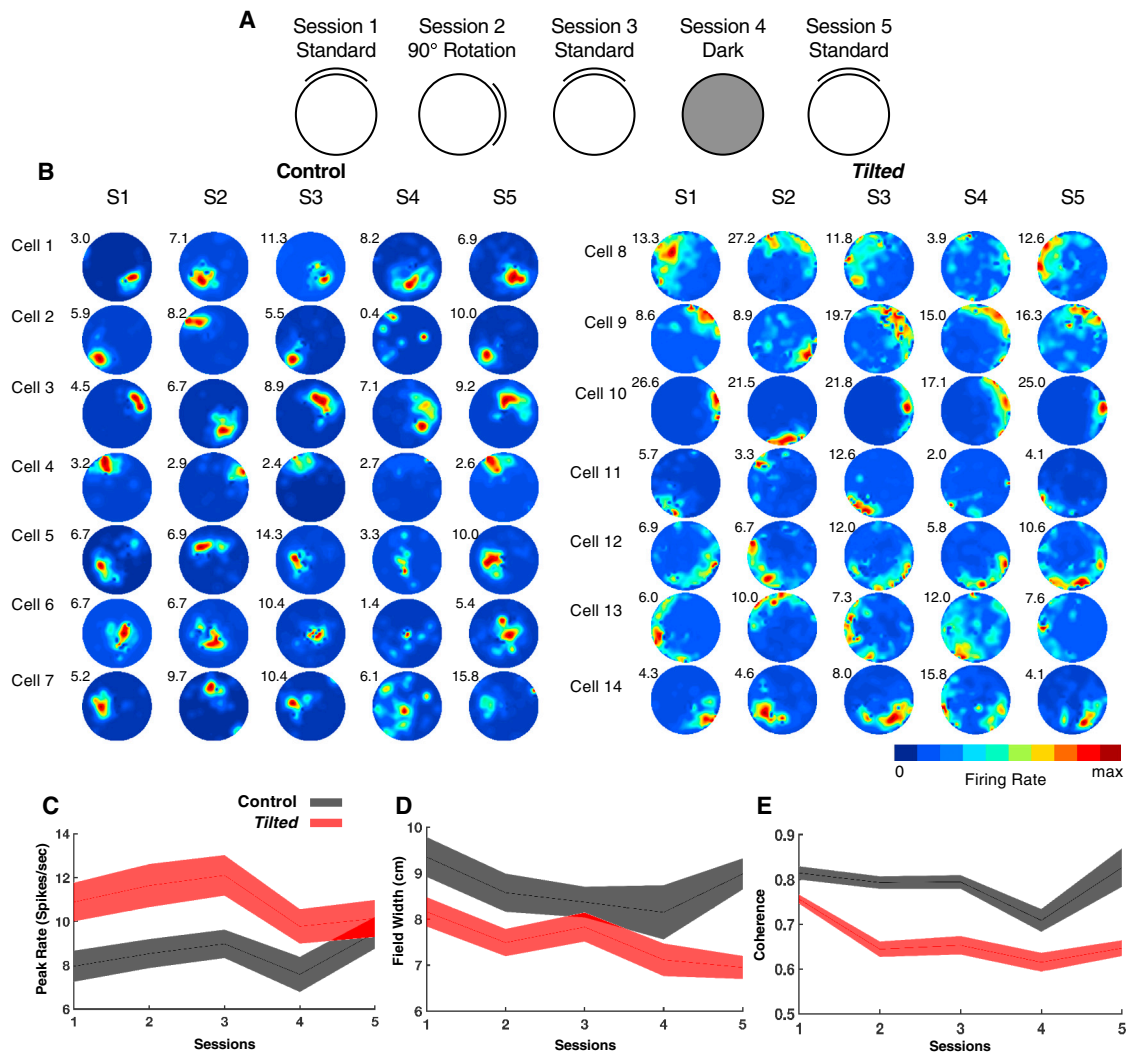


Figure 1. Overview of Experimental Design, Place-Cell Examples, and Basic Firing Characteristics

(A) Depiction of recording procedure across five recording sessions: Session 1, cue card was positioned in the standard north position; Session 2, cue card was rotated 90° clockwise or counterclockwise from the standard location; Session 3, cue card was returned to the standard location; Session 4, cue card was removed, and overhead lights were extinguished; and Session 5, white cue card was replaced at the standard location, and lights were turned on.

(B) Representative place cells from control (cells 1–7) and *tilted* (cells 8–14) mice over five sessions. Numbers at the top left of each rate map represent peak firing rate (Hz). Also see Figure S2.

(C) Plot showing the peak firing rate (spikes/second) for each place cell recorded in *tilted* and control mice with values from all sessions included.

(D) Plot showing the field width (cm) for each place cell recorded in *tilted* and control mice with values from all sessions included.

(E) Plot showing coherence measures for each place cell recorded in *tilted* and control mice with values from all sessions included. Also see Figure S3.

(C–E): Shaded error bars represent SEM. Also see Table S1.

population of place cells. Note that the fields from *tilted* mice appear to lack smoothness. These findings suggest that place cells from *tilted* mice covered a similar surface area of the arena to that of controls, but their fields had decreased coherence compared to control fields.

Spatial Distribution of Place-Cell Firing

Given that self-motion processing is disrupted in *tilted* mice, we hypothesized that place cells would be reliant on boundaries of the environment, resulting in an altered spatial distribution of place fields. Place fields from control mice were normally distributed throughout the arena, but most place fields from *tilted* mice

formed along the walls of the environment (Figure 2A). The mean field-to-wall distance (Figure 2B) and the peak firing bin-to-wall distance were shorter in *tilted* mice compared to control mice ($t(152) = 3.61$, $p < 0.001$, $CI[0.53, 1.82]$, $d = 0.61$; $t(87) = 5.09$, $p < 0.001$, $CI[1.63, 3.73]$, $d = 0.93$), suggesting that fields in *tilted* mice clustered near boundaries, whereas fields from control mice were normally distributed across the environment. We then calculated a border score (–1 to 1, with 1 representing fields in direct proximity to a boundary). Fields from *tilted* mice had higher border scores than control fields ($Z = -3.23$, $p = 0.001$, $d = -0.56$), had a larger proportion of border scores above 0 than controls ($\chi^2(1, 154) = 12.87$, $p < 0.001$), and were more

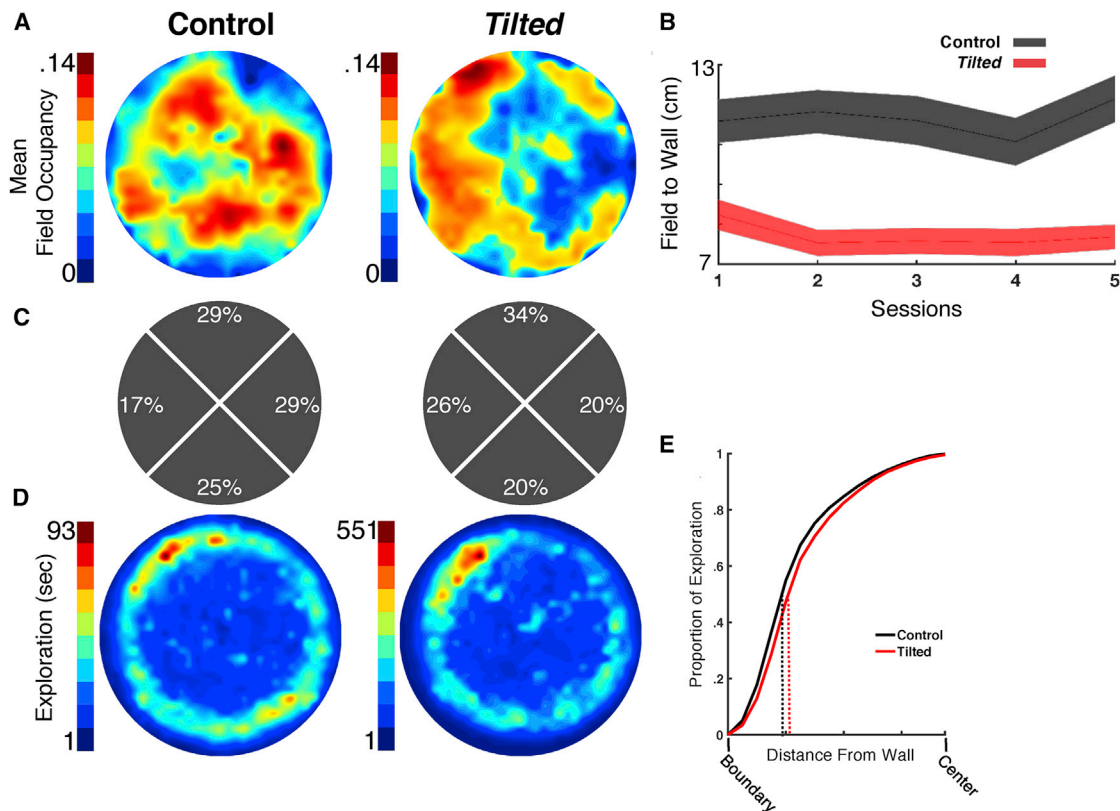


Figure 2. Place Cell Firing in *Tilted* Mice Is More Concentrated near Environmental Boundaries

(A) Place-field occupancy of all place cells recorded in control and *tilted* mice. Blue represents a lower place-field occupancy, and red represents a high place-field occupancy. Note that place cells from *tilted* mice appear to cluster closer to the cylinder boundaries compared to control mice. (B) Field-to-wall measures (cm) for place cells from control and *tilted* mice. Note that place fields from control mice form further from environmental boundaries than *tilted* mice. Shaded error bars represent SEM. (C) Percentage of place fields from control and *tilted* mice in each of four quadrants of the circular arena. (D) Occupancy of environmental sampling. (E) Proportion of exploration as a function of distance to the boundary. Note that *tilted* mice had similar occupancy compared to control mice, with the majority of exploration occurring near the boundary (within 10 cm), as illustrated by dotted lines at the 50% point.

likely to form close to boundaries than those from control mice overall ($F(1,146) = 32.93$, $p < 0.001$; Figure 2B), and this difference was stable across sessions within groups ($F(4,585) = 1.42$, $p = 0.227$). Together, these findings suggest that place cells from *tilted* mice are more likely to form along boundaries, which is likely due to the disruption in self-motion processing.

One explanation as to why place fields of *tilted* cells form near boundaries is that *tilted* mice may disproportionately explore near boundaries while neglecting the center of the arena. To rule out sampling bias, we analyzed environmental exploration and found that both groups occupied similar regions of the cylinder ($t(32) = 0.21$, $p = 0.835$; Figures 2D and 2E). Another possible explanation is that *tilted* cells disproportionately form fields near the cue card; however, after analyzing the spatial location of each firing field, we found a non-significant trending bias in firing locations ($\chi^2(1,154) = 13.72$, $p = 0.056$; Figure 2C).

Landmark Control

The ability of place cells to consistently fire in relation to external cues is thought to be derived from the head-direction cell system [18–21], and the preferred firing locations and directions of place

cells and head direction cells remain coupled to each other even when they become uncoupled from external landmarks [22]. Because head-direction cell activity and landmark navigation is known to be disrupted in *tilted* mice [7, 9], we assessed landmark control over place-cell activity by rotating the cue card in session 2 and measuring the degree to which place cells were anchored to that cue.

Place cells from both groups were influenced by the 90° cue rotation, but *tilted* mice showed more variability than controls (central median test: $p = 0.005$, $p = 0.943$, med = 90°; test for equality of concentration parameters: control $\kappa = 3.06$ and *tilted* $\kappa = 1.11$; Fr = 17.01, $p < 0.001$; Figure 3A). Figure 3B depicts the proportion of cells that rotated coherently with the landmark, the proportion that did not rotate, and the proportion that rotated in a direction inconsistent with the cue. The majority of cells in both groups maintained fields that rotated in the same direction as the cue. However, a smaller proportion of *tilted* cells rotated with the cue, relative to control cells (control = 88%; *tilted* = 61%, $\chi^2(1, N = 141) = 19.19$, $p < 0.001$). Sub-populations of fields in both groups failed to rotate with the cue or rotated to a different direction from the expected 90° following the cue

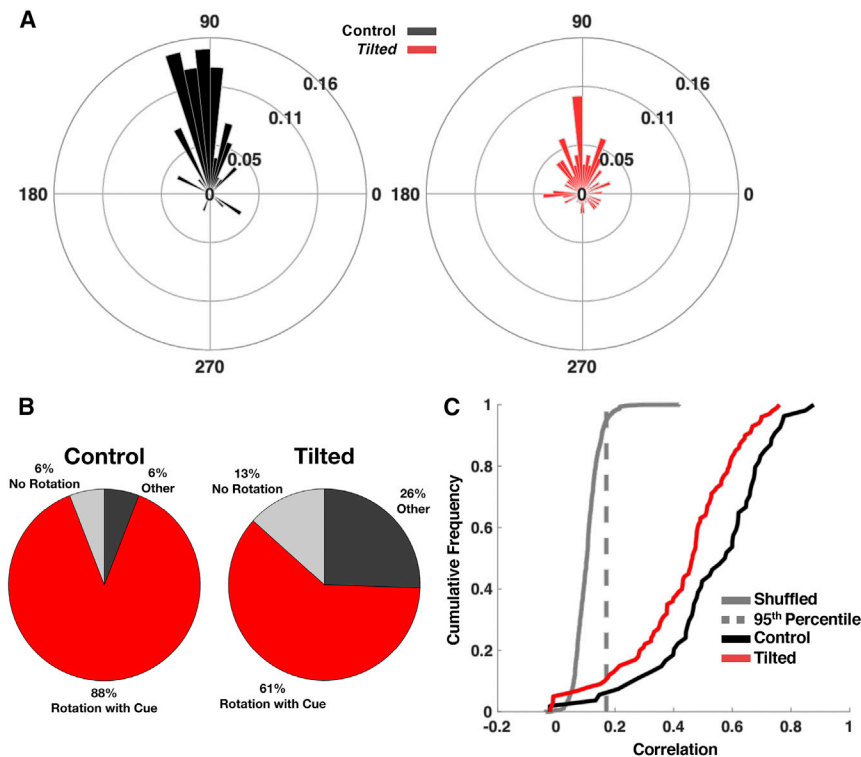


Figure 3. Landmark Control of Place Field following 90° Cue Rotation

(A) Polar plot depicting place-field rotation, normalized by probability, in 6° bins (black, control; red, *tilted*). Place-field rotation of 90° indicates that the cell's activity precisely rotated with the cue. Left: Control mice. Right: *Tilted* mice.

(B) Pie charts depicting percent of field anchoring following cue rotation.

(C) Cumulative density functions of cross-correlation values (r) following 90° cue rotation for place cells recorded in control (black) and *tilted* (red) mice. Shown are correlations following the rotation that maximized the correlation between session 1 and 2 rate maps. Fields from cue-rotation sessions were permuted to generate chance cross-correlations (gray line). The 95th percentile was then taken from the chance distribution and used as a threshold for evaluating the degree of field rotation in (A) (dashed gray line). Overall, *tilted* mice had lower cross-correlation values than control mice, indicating firing-field instability following cue rotation.

Stability of Firing Characteristics

Intra-trial stability was assessed through spatial correlations on rate maps from the first and second halves of each session (Figure 4A). *Tilted* place fields had

rotation. In control mice, 6% failed to rotate, and another 6% rotated in a different direction from the cue. However, 13% of *tilted* cells did not rotate with the cue, and 26% rotated in a different direction. These proportions were significantly different, ($\chi^2(1, N = 141) = 11.90, p = 0.002$). Additionally, spatial cross-correlations between session 1 and 2 suggest that place cells in *tilted* mice lacked spatial stability following the cue rotation. Specifically, spatial correlations between session 1 and 2, corrected for field rotation, from *tilted* mice were lower than those from controls ($t(152) = 3.38, p = 0.001, CI[0.04, 0.17], d = 0.57$; Figure 3C). Together, greater rotation variability, coupled with less accurate rotations with the cue, suggests that landmark control over place fields is impaired in *tilted* mice.

Spatial coherence was also affected by the cue rotation in *tilted* mice (Figure 1E). Coherence from *tilted* mice decreased throughout the first three sessions ($F(1, 142) = 34.99, p < 0.001$) and showed additional decreases from sessions 1 to 2 ($F(1, 143) = 33.17, p < 0.001$), and this decrease persisted through session 3 ($F(1, 142) = 25.75, p < 0.001$). In contrast, coherence of control fields was stable throughout these sessions ($F(1, 51) = 1.27, p = 0.26$). This finding further suggests that place fields from *tilted* mice were less reliable across sessions compared to control mice.

The increased variability in *tilted* place cells following the cue rotation may have resulted from reduced visual gaze control. Otoconia-deficient *head tilt* mice are known to have attenuated vestibulo-ocular reflex [23], and this deficit may be present in *tilted* mice. However, previous studies show that *tilted* mice are able to rely on their visual system to navigate to cues and that their performance suffers to a greater extent in non-visual environments or when visual cues are sparse [9, 24, 25].

lower intra-trial stability compared with controls overall ($F(1, 147) = 82.59, p < .001$; Figure 4B), suggesting that fields from *tilted* mice are unstable during short timescales. To further assess the stability of place-cell firing characteristics, standard sessions 1, 3, and 5 were separately analyzed as these sessions lacked the experimental interventions of sessions 2 and 4. However, sessions 3 and 5 were conducted directly after experimental-stimulus control sessions, and place fields may show carry-over effects from the preceding manipulations.

Control mice had stable coherence and peak bin-to-wall distances, and both groups had stable average firing rates, infield firing rates, number of active bins, information content, field-to-wall distances, and border scores across the three standard sessions (all $p \geq 0.11$; Table S1). However, place cells from *tilted* mice differed from controls in their peak firing rates ($F(2, 150) = 3.74, p = 0.026$, Figure 1C). Cells in both groups similarly increased in firing rate from session 1 to 3 ($F(1, 151) = 0.02, p = 0.897$), but *tilted* cells decreased in firing rate from session 3 to 5 compared with controls ($F(1, 151) = 6.50, p = 0.001$). These observations indicate that instability of firing rates occurred specifically after the dark session but did not occur after the cue-rotation sessions.

Field width of *tilted* place cells varied between standard sessions compared to controls ($F(2, 150) = 3.24, p = 0.041$; Figure 1D). Field widths from *tilted* cells decreased from session 3 to session 5, while field widths from control cells increased ($F(1, 151) = 6.51, p = 0.011$), suggesting that the dark session differentially affected place-field width between the two groups. However, both groups appeared to be slightly affected by the cue-rotation session and showed a similar ($F(1, 151) = 1.23, p = 0.269$) trending decrease (after Bonferroni correction) in field

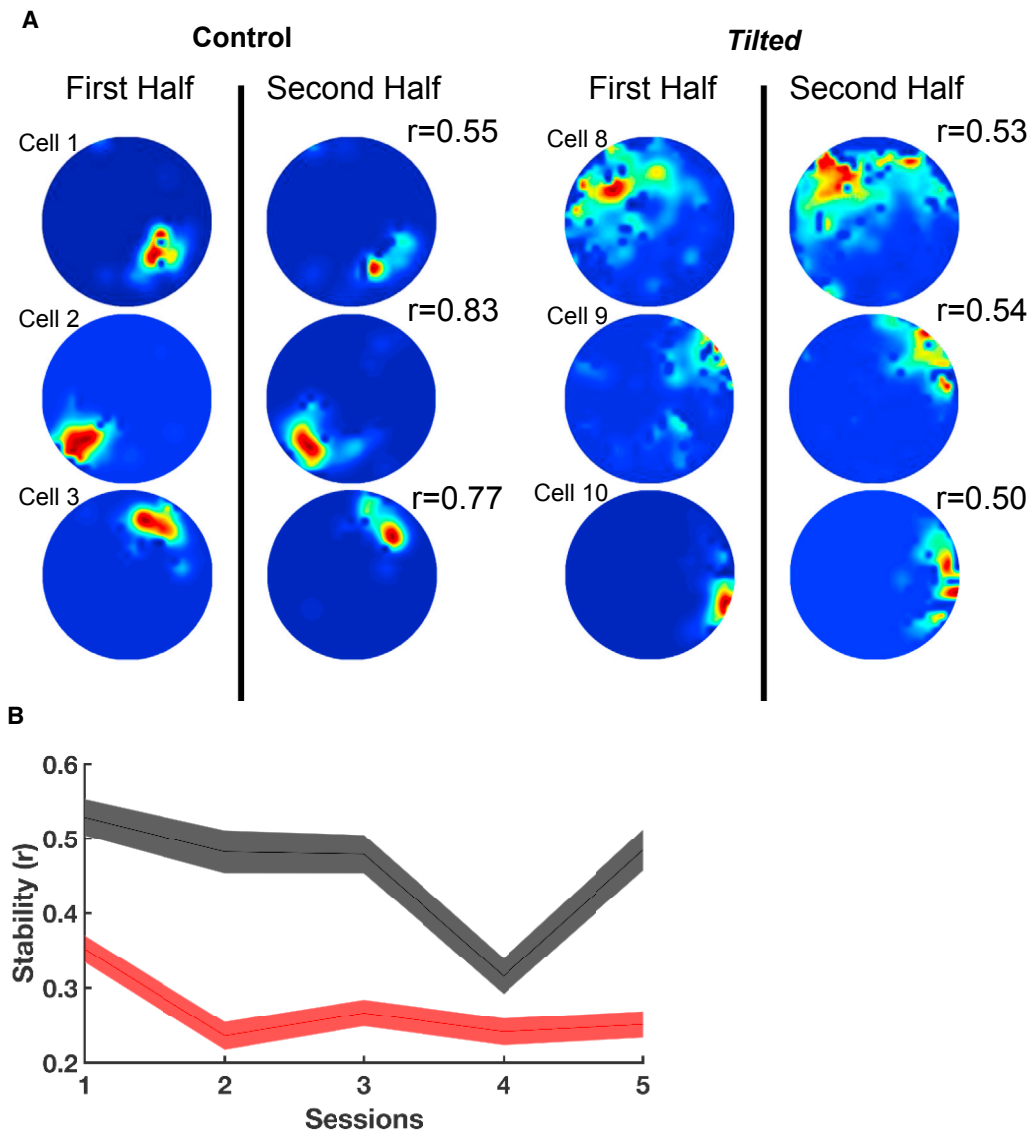


Figure 4. Intra-session Stability

(A) Rate maps depict the stability (r) between the first and second half of the first session using six example cells from Figure 1. Note that *tilted* cells appear to be less stable than control cells.

(B) Stability between groups over all sessions. Note that *tilted* mice have much lower stability compared to control mice for all sessions. Red, *tilted*; black: control; shaded lines represent SEM.

size between the first and second standard session ($F(1,151) = 4.82$, $p = 0.029$). Place fields from control mice recovered by session 5 ($F(1,53) = 0.90$, $p = 0.346$), while place fields from *tilted* mice further deteriorated in size ($F(1,99) = 9.71$, $p = 0.002$). Coupled with an overall decreased coherence, the data suggest that place fields from *tilted* mice became unstable over sessions even with repeated exposure to the same environment.

Spatial coherence of *tilted* place fields differed across standard sessions relative to controls ($F(2,141) = 5.64$, $p = 0.004$; Figure 1E). Coherence of *tilted* fields decreased from session 1 to 3, while coherence from controls stayed the same ($F(1,142) = 7.02$, $p = 0.008$), suggesting that the cue-rotation session differentially affected coherence among both groups. Further, coherence

in the *tilted* group remained low through standard session 5 ($F(1,143) = 8.71$, $p = 0.003$), which further suggests that the lack of self-motion cues causes decreased place-cell stability over sessions.

Place-Cell Stability Degrades in Darkness

Accurate navigation depends on non-visual external sensory information as well as internal self-motion cues [25, 26]. External sensory input can be derived from spatially arranged odor cues left behind during exploration [27], and place cells are able to maintain their field location in the dark on the basis of self-motion information [28]. Odor cues during exploration in the dark session were present in our experiment; however, we

expected a reduction in place-field stability in our *tilted* group due to their decrease in self-motion information.

Place cells between sessions 3 and 5 indicated differential changes in coherence in *tilted* cells ($F(2,137) = 4.59$, $p = 0.011$; Figure 1E). Surprisingly, control cells had a greater decrease from session 3 to 4 ($F(1,51) = 10.66$, $p = 0.001$) compared with *tilted* cells, which had no change in coherence ($F(1,86) = 1.96$, $p = 0.164$). There was also a similar finding in intra-trial stability. While control cells had a decrease in stability from session 3 to 4 ($F(1,50) = 27.20$, $p < 0.001$), *tilted* cells exhibited no change ($F(1,97) = 1.03$, $p = 0.311$; Figure 4B). The greater number of stable *tilted* cells may have resulted from a general reduction in stability, as place cells in *tilted* mice were already unstable in light before assessment during darkness. A similar conclusion was reached concerning head direction cells from *tilted* mice in darkness [7]. This finding suggests that *tilted* cells may be more reliant on cues other than vision, such as boundary information. Because self-motion cues in *tilted* mice might be generally unreliable in all conditions due to their inability to properly perceive linear acceleration, they may rely more on external cues, such as olfactory and tactile cues, and so were less affected by darkened conditions.

Effect of Otoconia Deficiency on CA1 and CA3 Neurons

Hippocampal areas CA1 and CA3 support distinct roles [29], which suggests that differences found in the present study may also differ between the regions. We therefore compared firing properties of place cells in session 1 between areas CA1 and CA3. First, coherence from *tilted* mice was lower in both sub-regions compared with controls ($p < 0.014$). Second, while CA1 place fields from *tilted* mice formed closer to boundaries compared with CA1 fields from controls (field to wall, peak to wall, border score all $p < 0.018$), CA3 place field from both groups did not differ in their field's relation to boundaries (field to wall, peak to wall, border score all $p > 0.118$). Although these results from CA3 were not significant, means from each measure suggest a tendency for *tilted* fields from CA3 to form along the walls (field to wall: control mean = 10.10 ± 0.78 , *tilted* mean = 8.64 ± 0.53 ; peak to wall: control mean = 7.81 ± 1.94 , *tilted* mean = 4.92 ± 0.75 ; border score: control mean = 0.23 ± 0.13 , *tilted* mean = 0.21 ± 0.09). Future work is needed to better understand the contribution of CA1 and CA3 in the formation of firing fields following vestibular dysfunction.

Conclusions

The present study revealed four novel conclusions regarding the relationship between the vestibular system and hippocampal place-cell function. First, hippocampal place cells in *tilted* mice express reductions in coherent firing activity, indicating a lack of smoothness of place-field firing. Second, place cells in *tilted* mice fired in close proximity to environmental boundaries, whereas control cells more evenly represented the entire environmental space. Third, *tilted* place cells showed decreases across a broad range of basic firing characteristics, including firing rate and field width, and the stability of these measures across repeated experiences in the same environment. Finally, *tilted* place cells do not lose firing coherence in the absence of

visual information, which suggests that they are more reliant on other inputs to maintain firing fields.

The present findings have many implications for spatial behavior and memory. It was previously reported that signals from the otolith organs are necessary for accurate homing performance in light and especially in darkness [25], for accurate navigational performance in radial environments [9], and for head-direction cell stability [7]. The present results show that otolith signals are also crucial for place-cell stability, and provides an explanation for the spatial memory deficits observed in behavioral experiments [9,25]. *Tilted* mice appear to be impaired at integrating information about linear self-motion, and their spatial memory acquisition, retention, and recall suffers when other cues are not available to help guide navigation.

STAR★METHODS

Detailed methods are provided in the online version of this paper and include the following:

- KEY RESOURCES TABLE
- CONTACT FOR REAGENT AND RESOURCE SHARING
- EXPERIMENTAL MODEL AND SUBJECT DETAILS
- METHOD DETAILS
 - Surgery
 - Electrodes
 - Apparatus
 - Recording procedure
 - Signal processing
 - Histology
- QUANTIFICATION AND STATISTICAL ANALYSIS
 - Spatial rate map construction
 - Information Content & Coherence
 - Sparsity
 - Cell type identification
 - Intra-Trial Stability
 - Mean Rate Maps
 - Environmental Occupancy
 - Place Field Clustering in Relation to Cue Card
 - Shuffling
 - Firing field Boundaries
 - Border Score
 - Cue Card Rotation Test
 - Spike-train Theta Modulation
 - Group Comparisons
- DATA AND SOFTWARE AVAILABILITY

SUPPLEMENTAL INFORMATION

Supplemental Information includes three figures and one table and can be found with this article online at <https://doi.org/10.1016/j.cub.2018.04.034>.

ACKNOWLEDGMENTS

This research was supported by NIDCD grant R15DC012630 to R.M.Y., NIAAA grant R21AA024983 and pilot project grant P50AA022534 to B.J.C., and NIAAA grant T32AA014127-15 to R.E.H. The authors thank Laura Berkowitz, Lucas Carstensen, Morgan Hardwick, and Seth Kirby for assistance with data and statistical analyses.

AUTHOR CONTRIBUTIONS

Conceptualization, R.M.Y. and B.J.C.; Methodology, R.M.Y.; Software, J.J.S. and R.E.H.; Validation, J.J.S.; Formal Analysis, R.E.H. and J.J.S.; Investigation, S.A.R. and R.E.H.; Resources, R.M.Y.; Data Curation, R.E.H. and S.A.R.; Writing – Original Draft, R.E.H.; Writing – Review & Editing, B.J.C., R.M.Y., and R.E.H.; Visualization, R.E.H. and G.R.W.; Supervision, R.M.Y.; Project Administration, R.M.Y.; Funding Acquisition, R.M.Y.

DECLARATION OF INTERESTS

The authors declare no competing interests.

Received: October 19, 2017

Revised: February 1, 2018

Accepted: April 11, 2018

Published: May 17, 2018

REFERENCES

- O'Keefe, J., and Dostrovsky, J. (1971). The hippocampus as a spatial map. Preliminary evidence from unit activity in the freely-moving rat. *Brain Res.* 34, 171–175.
- McNaughton, B.L., Knierim, J.J., and Wilson, M.A. (1995). *The Cognitive Neurosciences* (Cambridge, Massachusetts: Massachusetts Institute of Technology).
- Russell, N.A., Horii, A., Smith, P.F., Darlington, C.L., and Bilkey, D.K. (2003). Long-term effects of permanent vestibular lesions on hippocampal spatial firing. *J. Neurosci.* 23, 6490–6498.
- Stackman, R.W., Clark, A.S., and Taube, J.S. (2002). Hippocampal spatial representations require vestibular input. *Hippocampus* 12, 291–303.
- Stackman, R.W., and Taube, J.S. (1997). Firing properties of head direction cells in the rat anterior thalamic nucleus: dependence on vestibular input. *J. Neurosci.* 17, 4349–4358.
- Yoder, R.M., and Taube, J.S. (2014). The vestibular contribution to the head direction signal and navigation. *Front. Integr. Neurosci* 8, <https://doi.org/10.3389/fnint.2014.00032>.
- Yoder, R.M., and Taube, J.S. (2009). Head direction cell activity in mice: robust directional signal depends on intact otolith organs. *J. Neurosci.* 29, 1061–1076.
- Harvey, R.E., Thompson, S.M., Sanchez, L.M., Yoder, R.M., and Clark, B.J. (2017). Post-training inactivation of the anterior thalamic nuclei impairs spatial performance on the radial arm maze. *Front. Neurosci.* 11, 94.
- Yoder, R.M., and Kirby, S.L. (2014). Otoconia-deficient mice show selective spatial deficits. *Hippocampus* 24, 1169–1177.
- Calton, J.L., Stackman, R.W., Goodridge, J.P., Archey, W.B., Dudchenko, P.A., and Taube, J.S. (2003). Hippocampal place cell instability after lesions of the head direction cell network. *J. Neurosci.* 23, 9719–9731.
- Clark, B.J., and Harvey, R.E. (2016). Do the anterior and lateral thalamic nuclei make distinct contributions to spatial representation and memory? *Neurobiol. Learn. Mem.* 133, 69–78.
- Harland, B., Grieves, R.M., Bett, D., Stentiford, R., Wood, E.R., and Dudchenko, P.A. (2017). Lesions of the head direction cell system increase hippocampal place field repetition. *Curr. Biol.* 27, 2706–2712.e2.
- Winter, S.S., Clark, B.J., and Taube, J.S. (2015). Spatial navigation. Disruption of the head direction cell network impairs the parahippocampal grid cell signal. *Science* 347, 870–874.
- Yoder, R.M., Clark, B.J., and Taube, J.S. (2011). Origins of landmark encoding in the brain. *Trends Neurosci.* 34, 561–571.
- Terrazas, A., Krause, M., Lipa, P., Gothard, K.M., Barnes, C.A., and McNaughton, B.L. (2005). Self-motion and the hippocampal spatial metric. *J. Neurosci.* 25, 8085–8096.
- Buzsáki, G. (2002). Theta oscillations in the hippocampus. *Neuron* 33, 325–340.
- Yartsev, M.M., Witter, M.P., and Ulanovsky, N. (2011). Grid cells without theta oscillations in the entorhinal cortex of bats. *Nature* 479, 103–107.
- McNaughton, B.L., Barnes, C.A., Gerrard, J.L., Gothard, K., Jung, M.W., Knierim, J.J., Kudrimoti, H., Qin, Y., Skaggs, W.E., Suster, M., and Weaver, K.L. (1996). Deciphering the hippocampal polyglot: the hippocampus as a path integration system. *J. Exp. Biol.* 199, 173–185.
- Muller, R.U., Ranck, J.B., Jr., and Taube, J.S. (1996). Head direction cells: properties and functional significance. *Curr. Opin. Neurobiol.* 6, 196–206.
- O'Keefe, J., and Burgess, N. (1996). Geometric determinants of the place fields of hippocampal neurons. *Nature* 381, 425–428.
- Yoganarasimha, D., and Knierim, J.J. (2005). Coupling between place cells and head direction cells during relative translations and rotations of distal landmarks. *Exp. Brain Res.* 160, 344–359.
- Knierim, J.J., Kudrimoti, H.S., and McNaughton, B.L. (1995). Place cells, head direction cells, and the learning of landmark stability. *J. Neurosci.* 15, 1648–1659.
- Harrod, C.G., and Baker, J.F. (2003). The vestibulo ocular reflex (VOR) in otoconia deficient head tilt (het) mutant mice versus wild type C57BL/6 mice. *Brain Res.* 972, 75–83.
- Blankenship, P.A., Cherep, L.A., Donaldson, T.N., Brockman, S.N., Trainer, A.D., Yoder, R.M., and Wallace, D.G. (2017). Otolith dysfunction alters exploratory movement in mice. *Behav. Brain Res.* 325 (Pt A), 1–11.
- Yoder, R.M., Goebel, E.A., Köppen, J.R., Blankenship, P.A., Blackwell, A.A., and Wallace, D.G. (2015). Otolithic information is required for homing in the mouse. *Hippocampus* 25, 890–899.
- Wallace, D.G., Hines, D.J., Pellis, S.M., and Whishaw, I.Q. (2002). Vestibular information is required for dead reckoning in the rat. *J. Neurosci.* 22, 10009–10017.
- Zhang, S., and Manahan-Vaughan, D. (2015). Spatial olfactory learning contributes to place field formation in the hippocampus. *Cereb. Cortex* 25, 423–432.
- Quirk, G.J., Muller, R.U., and Kubie, J.L. (1990). The firing of hippocampal place cells in the dark depends on the rat's recent experience. *J. Neurosci.* 10, 2008–2017.
- Mizuseki, K., Royer, S., Diba, K., and Buzsáki, G. (2012). Activity dynamics and behavioral correlates of CA3 and CA1 hippocampal pyramidal neurons. *Hippocampus* 22, 1659–1680.
- Ornitz, D.M., Bohne, B.A., Thalmann, I., Harding, G.W., and Thalmann, R. (1998). Otoconial agenesis in tilted mutant mice. *Hear. Res.* 122, 60–70.
- Gray, C.M., Maldonado, P.E., Wilson, M., and McNaughton, B. (1995). Tetrodes markedly improve the reliability and yield of multiple single-unit isolation from multi-unit recordings in cat striate cortex. *J. Neurosci. Methods* 63, 43–54.
- McNaughton, B.L., O'Keefe, J., and Barnes, C.A. (1983). The stereotrode: a new technique for simultaneous isolation of several single units in the central nervous system from multiple unit records. *J. Neurosci. Methods* 8, 391–397.
- Siegel, J.J., Neunuebel, J.P., and Knierim, J.J. (2008). Dominance of the proximal coordinate frame in determining the locations of hippocampal place cell activity during navigation. *J. Neurophysiol.* 99, 60–76.
- Siegel, J.J., Nitz, D., and Bingman, V.P. (2005). Spatial-specificity of single-units in the hippocampal formation of freely moving homing pigeons. *Hippocampus* 15, 26–40.
- Siegel, J.J., Nitz, D., and Bingman, V.P. (2006). Lateralized functional components of spatial cognition in the avian hippocampal formation: evidence from single-unit recordings in freely moving homing pigeons. *Hippocampus* 16, 125–140.
- Skaggs, W., McNaughton, B., Gothard, K., and Markus, E. (1992). An information-theoretic approach to deciphering the hippocampal code. *Proceedings of the Advances in Neural Information Processing Systems Conference (NIPS)*, pp. 1030–1037.
- Fox, S.E., and Ranck, J.B., Jr. (1981). Electrophysiological characteristics of hippocampal complex-spike cells and theta cells. *Exp. Brain Res.* 41, 399–410.

38. Frank, L.M., Brown, E.N., and Wilson, M.A. (2001). A comparison of the firing properties of putative excitatory and inhibitory neurons from CA1 and the entorhinal cortex. *J. Neurophysiol.* *86*, 2029–2040.
39. Hargreaves, E.L., Rao, G., Lee, I., and Knierim, J.J. (2005). Major dissociation between medial and lateral entorhinal input to dorsal hippocampus. *Science* *308*, 1792–1794.
40. Solstad, T., Boccara, C.N., Kropff, E., Moser, M.-B., and Moser, E.I. (2008). Representation of geometric borders in the entorhinal cortex. *Science* *322*, 1865–1868.
41. Muller, R.U., and Kubie, J.L. (1987). The effects of changes in the environment on the spatial firing of hippocampal complex-spike cells. *J. Neurosci.* *7*, 1951–1968.
42. Boccara, C.N., Sargolini, F., Thoresen, V.H., Solstad, T., Witter, M.P., Moser, E.I., and Moser, M.-B. (2010). Grid cells in pre- and parasubiculum. *Nat. Neurosci.* *13*, 987–994.
43. Deshmukh, S.S., Yoganarasimha, D., Voicu, H., and Knierim, J.J. (2010). Theta modulation in the medial and the lateral entorhinal cortices. *J. Neurophysiol.* *104*, 994–1006.
44. Langston, R.F., Ainge, J.A., Couey, J.J., Canto, C.B., Bjerknes, T.L., Witter, M.P., Moser, E.I., and Moser, M.-B. (2010). Development of the spatial representation system in the rat. *Science* *328*, 1576–1580.
45. Wills, T.J., Cacucci, F., Burgess, N., and O'Keefe, J. (2010). Development of the hippocampal cognitive map in preweanling rats. *Science* *328*, 1573–1576.

STAR★METHODS

KEY RESOURCES TABLE

REAGENT or RESOURCE	SOURCE	IDENTIFIER
Chemicals, Peptides, and Recombinant Proteins		
ketamine	Midwest Veterinary	N/A
xylazine	Midwest Veterinary	N/A
Buprenorphine	Midwest Veterinary	N/A
Experimental Models: Organisms/Strains		
C57BL/6J mice	Jackson; bred in-house	RRID:IMSR_JAX:000664
B6.Cg- <i>Otop1^{fl}/J</i> mice	Jackson; bred in-house	RRID:IMSR_JAX: 001104
Software and Algorithms		
Spike Sort 3D	Neuralynx	N/A
Igor Pro	Wavemetrics	N/A
MATLAB v 2016b	MathWorks	N/A
Statistics Toolbox for MATLAB	MathWorks	N/A
Other		
Electrodes	Custom Built	N/A
Digital Neuralynx recording system, Lynx SX	Neuralynx	N/A

CONTACT FOR REAGENT AND RESOURCE SHARING

Further information and requests for resources and reagents should be directed to and will be fulfilled by the Lead Contact, Ryan Yoder (ryoder@coastal.edu).

EXPERIMENTAL MODEL AND SUBJECT DETAILS

All procedures involving live animals were approved by the Purdue Animal Care & Use Committee. Control ($n = 3$) and *tilted* ($n = 7$) adult male mice, age 3–8 mo. at the start of the study, were pseudo randomly selected from the descendants of mice purchased from Jackson Laboratories (Bar Harbor, ME). The initial stock of *tilted* mice was bred to produce offspring that were homozygous ($-/-$) for the recessive mutation, or crossed with C57BL/6J mice to produce offspring that were heterozygous ($+/-$) for the mutation. The F1 $+/-$ and $-/-$ mice were then bred to produce $+/-$ and $-/-$ offspring, with a predicted 50% frequency of each genotype. A swim test was used to determine whether mice were $+/-$ or $-/-$, as described previously [7, 9, 24, 25, 30]. Subsequent generations were produced by breeding $+/-$ and $-/-$ mice.

METHOD DETAILS

Surgery

Mice were anesthetized with ketamine/xylazine (90 and 10 mg/kg, respectively) and positioned in a stereotaxic apparatus (David Kopf Instruments) with bregma and lambda in the same plane. The scalp was retracted and a hole was drilled above the hippocampus. Six additional holes were drilled in the frontal, parietal, and occipital bones to hold jeweler's screws (Lomat Precision, Montreal, Quebec, Canada). These screws were reinforced to the skull with a drop of sterile cyanoacrylate. With the tetrode bundle positioned dorsal to hippocampus (1.5 mm posterior, 1.50 mm lateral, 0.5 mm ventral to bregma), the drive screws/cuff assemblies were fastened to the skull and jeweler's screws with Grip Cement (Dentsply International). The scalp was sutured around the electrode drive and the wound was covered with Neosporin. Buprenorphine (0.015 mg/kg) was administered every 12 hours as a postoperative analgesic for the following 48 hours, and the animal was allowed to recover at least 1 week before recording.

Electrodes

Electrode design was based on a design used previously with mice [7]. Each microdrive contained four tetrodes constructed from Teflon-insulated 16- μ m nichrome wires, with gold-plated tips (tip impedance \sim 200 k Ω), and a single stainless steel ground wire (50 μ m; California Fine Wire). The four tetrodes were encased by a 26 gauge stainless steel cannula, and each wire contacted one gold pin of an electrode interface board (EIB-18, Neuralynx, Bozeman, MT). The electrode interface board and wires were

then cemented together with dental acrylic, and then attached to three drive screws. Custom-built threaded plastic cuffs were then threaded onto the drive screws. The tetrodes and cannula were then sterilized prior to surgical procedures.

Apparatus

The recording arena consisted of a black cylinder (61 cm diameter) positioned on a black formica tabletop (40 cm height). A white cue card covered $\sim 90^\circ$ of the wall surface, with the bottom edge ~ 10 cm above the floor to prevent mice from using the card as a tactile cue. For standard trials, the cue card was centered at the 9:00 position as viewed by the camera. The entire arena was located within a large wooden box (122.5 cm \times 122.5 cm \times 191 cm high) with black walls and ceiling. Four dimmable incandescent lights (25W) mounted on the ceiling provided illumination.

Recording procedure

Electrical activity was recorded daily from all tetrodes, across five recording sessions: (1) *standard 1*, cue card was positioned in the standard position; (2) *rotation*, cue card was rotated 90° clockwise (CW) or counterclockwise (CCW) from the standard location; (3) *standard 2*, cue card was returned to the standard location; (4) *darkness*, cue card was removed and overhead lights were extinguished; and (5) *standard 3*, white cue card was replaced at the standard location and lights were turned on (Figure 1A). Before the beginning of each session, the arena floor was cleaned with alcohol to discourage the use of olfactory cues. The mouse was then placed in an opaque container and the experimenter slowly rotated the animal in both directions to disorient the animal before it was lowered into the arena, [7]. Recording sessions were 15 to 30 minutes in duration, as necessary, to obtain adequate sampling of all locations within the arena. Each day at the end of recording, the tetrode bundle was advanced ~ 50 μm to approach a putatively different set of neurons (tetrode penetrations shown for each animal in Figure S1). This process was repeated until well separated cells were no longer identifiable, and theta rhythm was not seen in the local field potential.

Signal processing

Thresholded waveforms from each tetrode were conducted to a 16-channel head stage containing an operational amplifier (Neuralynx). A flexible cable connected the head stage to a 32-ch Digital Lynx data acquisition system (Neuralynx), where electrical signals were acquired at 32 kHz. An overhead color video camera was used to monitor the animal's position at 30 frames/sec by tracking the position of one red light-emitting diode (LED) attached to the animal's head stage. The positions of the LED during adjacent 33.3 msec epochs were then interpolated to estimate the LED position at 16.67 msec intervals, to mimic 60 frames/sec temporal resolution.

Tetrode signals were analyzed offline with SpikeSort 3D (Neuralynx). Signals from each tetrode were then evaluated for event parameters that correspond to the activity of a single neuron, using a procedure known as "cluster cutting" [31, 32]. Timestamps associated with single-unit events were then matched to the associated 16.67 msec interval from the video record using custom analysis software.

Histology

At the end of electrophysiological recording procedures, mice were deeply anesthetized with isoflurane and electrode tip locations were marked by a small lesion created by applying constant current (15 μA , 20 s). Mice were then killed by transcardial perfusion with normal saline followed by 10% Formalin, and brains were then placed in Formalin overnight to ensure adequate fixation. Brains were then placed in 20% sucrose for cryoprotection before they were sectioned at 40 μm on a freezing microtome. Brain sections containing the hippocampus were mounted on gelatin-coated microscope slides and stained with Cresyl violet. Electrode position at the time of each recording was estimated relative to the site of the final electrode tip location (example tetrode penetrations shown in Figure S1A & reconstruction of electrode tracks from all mice is shown in Figure S1B); our analyses included only sessions where the electrode tip was estimated to be located between the dorsal limit of area CA1 and the ventral limit of CA3, or the dorsal and ventral limits of CA3. We then categorized the recordings to have occurred either from CA1 or CA3; however, it is important to note the possibility that a small number of recordings may have included granule cells from the dentate subregion, given its proximity to CA3.

QUANTIFICATION AND STATISTICAL ANALYSIS

Spatial rate map construction

Rate maps were constructed and initial firing characteristics (average and peak firing rate, information content, and coherence) were calculated using custom scripts in Igor Pro (WaveMetrics, Portland, OR). The location-specific activity of each single unit was assessed by first creating a two-dimensional firing rate map for each of the 5 trials on a given day (standard configuration, cue rotation, standard, dark condition, standard). Each firing rate map was created by dividing the camera image into a 64×48 array (2.44 cm per pixel) and calculating the average firing rate (total number of spikes/total dwell time) for each pixel of the array. Pixels with a dwell time < 100 ms were excluded from all analyses. Epochs in which spike data were recorded in the absence of position data (e.g., if a gap occurred in tracking due to rearing, for example) were excluded from analysis. The resulting firing rate maps were gently smoothed with a conditional algorithm using a 5×5 hybrid box filter (Igor Pro, WaveMetrics). If ≥ 100 spikes contributed to a given rate map the filter was passed five times; if < 100 spikes were included, the filter was passed ten times. Passing the box filter

additional times for low-firing-rate cells better preserved the size and shape of the place fields compared to increasing the size of the smoothing kernel [33–35].

Information Content & Coherence

Two measures were used to evaluate the location-specific activity of each rate map. First, spatial information (in bits/pixel) was calculated as previously described; $I = [-\sum_x P_x(\lambda_x/\lambda) \log_2(\lambda_x/\lambda)]$ where λ is the mean firing rate of the cell, λ_x is the mean firing rate while the animal is occupying bin x , and P_x is the probability of occupancy for bin x [36]. A high spatial information score indicated strong location-specific activity with little out-of-field spiking. Second, spatial coherence was used as a measure of rate map quality by calculating the correlation (Pearson r) between the average firing rate for each pixel of the smoothed rate map with the average of the surrounding 8 pixels (see Figure S3 for coherence measures calculated on the raw rate maps). Rate maps with place fields having smooth transition gradients with low out-of-field activity have high spatial coherence, while rate maps with packets of sporadic activity across the environment or that lack place fields will have low spatial coherence scores.

Sparsity

Sparsity, which indicates the relative proportion of the maze on which the cell fired, was calculated using formula: $\text{sparsity} = \sum (P_i \cdot R_i^2) / R^2$ where P_i is the probability of occupancy of bin i , R_i is the mean firing rate in bin i , and R is the overall mean firing rate. A sparsity score of 0.10 would indicate that the cell fired on 10% of the maze surface.

Cell type identification

Only well-isolated units with at least 100 spikes during the first recording session were included in the study. Neurons were classified as place cells if they exhibited good spatial selectivity based on independent visual inspection of the rate map, and by using a combination of spatial information content score ≥ 0.60 , and spatial coherence score ≥ 0.50 . Two cells (1 from control and 1 from *tilted* animals) that had spatial information content and coherence values below the criteria in the first session were classified as place cells, based on visual inspection of their rate maps, and were therefore included in the study. We confirmed that our sample of place cells did not contain fast spiking interneurons by identifying and eliminating interneurons based on short peak to valley spike widths ($< 200 \mu\text{s}$) and high average firing rates ($> 10\text{Hz}$) [37–39]. Example waveforms are shown in Figure S1. Out of the 422 neurons recorded neurons from control mice, 146 were classified as putative pyramidal cells and, of those, 54 met the criteria to be classified as place cells (36.99%). Out of the 1226 neurons recorded from *tilted* mice, 370 were classified as putative pyramidal cells and, of those, 100 neurons met the criteria to be classified as place cells (27.03%). Example place cell rate maps from both groups shown in Figure 1B, Figure S2 illustrates where these examples reside with respect to the population of principle cells, and Figure S1 characterizes our full population of pyramidal cells in terms of coherence and information content.

Intra-Trial Stability

Intra-trial stability was assessed by calculating the correlation coefficient between rate maps created from the first and second halves of a session.

Mean Rate Maps

To create mean field occupancy maps for Figure 2A, all session 1 rate maps that passed the criteria for containing place fields were compiled. Maps were then normalized by their peak firing rate from 0 to 1 and all maps were averaged together for each group.

Environmental Occupancy

To assess each group's ability to fully sample the circular environment, we first created binned (2.44 cm per bin) occupancy maps from the cumulative locomotor path for each group, shown in Figure 2D. Next, to quantify their occupancy along the edge versus the center of the enclosure, we first created an annulus with the same radius as the cylinder and calculated the proportion of path occupying the annulus and cylinder boundary. This initial calculation gave us a proportion of 0 as the distance between the annulus and boundary was 0 cm. We then reduced the annulus's radius by 5% (3.05cm) and recalculated the proportion of path occupying that region of the cylinder. We repeated this process of increasing the distance between the edge of the annulus and cylinder boundary until the annulus had a radius of 0 cm. Thus, the resulting data represents the proportion of locomotor path as a function of distance from the environmental boundary, and this data is shown in Figure 2E.

Place Field Clustering in Relation to Cue Card

To assess bias in place field clustering in relation to the cue card, we analyzed firing field clustering by dividing the arena into 4 quadrants shown in Figure 2C and labeling which quadrant fields were in. After firing field boundaries were identified, the four quadrants were divided and the numbers of bins from the firing field was summed per quadrant. The quadrant with the highest number of bins was considered the quadrant that contained the firing field. This process was repeated for all cells, and proportions per quadrant were calculated to assess if a bias existed.

Shuffling

We generated a shuffled distribution to assess a lower cut off for rotated field cross correlations. This procedure was conducted as cells would sometimes become unstable during the cue rotation session. With a lower correlation cut-off of 0.17, 5.5% of control cells and 10% of *tilted* cells were not included in the subsequent analysis of cue rotation. Importantly, the proportion of cells eliminated did not differ significantly between groups, $\chi^2(1, N = 154) = 0.90, p = 0.344$. To carry out this procedure, bins from each rate map from the second session were randomly shuffled and then field rotation correlation was calculated (as described in Data analysis: Field Rotation). This procedure was carried out 400 times per cell and the resulting correlations were pooled to create a shuffled distribution from which a 95th percentile could be obtained. This percentile was then used as a lower cut off to assess field rotation as described above (Data analysis: Field Rotation).

Firing field Boundaries

Firing fields were located by first locating the peak bin and then expanding outward while including bins at least 0.2 times that of the peak rate and repeating this process at each new bin included in the field. If any edge of the field came upon a bin that was not 0.2 times, that bin was not counted in the field. This recursive process was ended once no more contiguous bins passing that threshold were found. If the resultant field was less than 10 bins (24.40² cm) in total, the next highest peak bin was then defined and the procedure was repeated. This process was then repeated until an optimal field of all the above characteristics was defined. Important to note, only the maximum firing field from a cell with multiple fields was taken.

Border Score

To identify place cells with firing characteristics closely associated with the environmental boundaries, a border score was calculated from each rate map. A border score measures the firing localized to the boundaries of an environment as compared to the firing within the center of the environment [40]. First, firing field boundaries were identified as described above (Data analysis: Firing field boundaries). Next, the number of bins along the border that the firing field occupied was defined as the value C_M . The mean firing distance dm was calculated as the average distance to the nearest wall of each bin in the map, weighted by its firing rate. Finally, the border score, given by $b = [C_M - dm / C_M + dm]$, ranged from -1 for cells with central firing to 1 for cells with firing in close proximity to the environment's boundaries.

Cue Card Rotation Test

We assessed the degree to which hippocampal place cells were controlled by environmental landmarks by rotating the cue card from its standard position by 90°. To evaluate the effects of cue rotation on place fields, a cross-correlation method was used [10, 41] in which the session 2 rate maps were rotated in 6° increments and cross correlated with the session 1 rate maps. The magnitude of rotation (in degrees) required to obtain the maximal correlation was considered to be the amount of rotation by the place field between session 1 and session 2. Proportion of field rotation was assessed by grouping the angular data in three groups: $\pm 45^\circ$ around 90° indicating “rotation with cue,” $\pm 45^\circ$ around 0° indicating “no rotation,” and $\pm 90^\circ$ around 225° indicating “other.”

Spike-train Theta Modulation

Because most neurons in the hippocampus are theta-modulated [16], we assessed the degree of theta modulation in the spiking patterns of place cells using spike-train temporal autocorrelograms similar to methods used by Yartsev, Witter, & Ulanovsky, (2011). With a bin size of 10 ms, temporal autocorrelograms were computed between ± 500 ms. The temporal power spectrum was then evaluated by computing a fast Fourier transform (FFT) of the autocorrelogram and calculating the square of the FFT magnitude. After smoothing the power spectrum with a 2-Hz rectangular window, the peak value in the 4-12 Hz theta band was identified. The mean power within 1Hz of each side of the peak theta frequency was then divided by the mean power between 0-50 Hz which resulted in an index similar to the theta index previously used in rat medial entorhinal cortex recordings to identify theta modulation of grid cells, [42–45]. To determine if cells were theta modulated, we performed a shuffling procedure on each spike-train. Cells with a theta index greater than or equal to the 95th percentile of their shuffled distribution were considered to be modulated by the theta frequency. This procedure determined that 30 of 54 control cells (56%) and 52 of 100 *tilted* cells (52%) were theta modulated. The peak theta frequencies from theta modulated cells were then compared between groups.

Group Comparisons

For each sample distribution, a Kolmogorov-Smirnov (KS) test was used to test the null hypothesis that the z-scored sample was derived from a standard normal distribution. If the KS null hypothesis failed rejection, a two-sample t test was used to test the sample mean. For each between-group comparison, a two-sample t test for equal or unequal variance was used to test equality of means only if both sample distributions failed KS test rejection. If at least one group passed the KS test, a Wilcoxon rank sum test was used to test the sample median. Effect size for all between groups two-sample comparisons were estimated using Cohen's D. All between groups comparisons of proportions were computed by Chi Square. Between groups and group by session comparisons were computed using mixed ANOVA. Simple effects were computed using either mixed or repeated-measures ANOVA. Results of mixed

ANOVAs are sometimes discussed separately. Multiple comparisons were corrected for the family-wise error rate with the Bonferroni procedure with a starting two-tailed $\alpha = 0.05$. The Central Median Test was used to test whether angular data were equally clustered around a central median, and the homogeneity of concentration test was used to test whether the angular shifts were distributed similarly between groups.

DATA AND SOFTWARE AVAILABILITY

Further information and requests for resources should be directed to and will be fulfilled by the Lead Contact, Ryan Yoder.